Electronic Research Archive

ERA, 31(7): 3915–3942.
DOI: 10.3934/era.2023199
Received: 13 March 2023
Revised: 18 April 2023
Accepted: 20 April 2023
Published: 15 May 2023

http://www.aimspress.com/journal/ERA

Research article

Fault location in a marine low speed two stroke diesel engine using the characteristic curves method

Nan Xu[1], Longbin Yang[1,*], Andrea Lazzaretto[2,*], Massimo Masi[3], Zhenyu Shen[1], YunPeng Fu[4] and JiaMeng Wang[4]

[1] College of Power and Energy Engineering, Harbin Engineering University, Harbin 150001, China
[2] Department of Industrial Engineering, University of Padova, Padova 35131, Italy
[3] Department of Management and Engineering, University of Padova, Padova 35131, Italy
[4] Dalian marine diesel CO., Ltd, Dalian 116083, China

* **Correspondence:** Email: yanglb@hrbeu.edu.cn, andrea.lazzaretto@unipd.it; Tel: +8613936138853, +393347151279.

Abstract: When a malfunction occurs in a marine main engine system, the impact of the anomaly will propagate through the system, affecting the performance of all relevant components in the system. The phenomenon of fault propagation in the system caused by induced factors can interfere with fault localization, making the latter a difficult task to solve. This paper aims at showing how the "characteristic curves method" is able to properly locate malfunctions also when more malfunctions appear simultaneously. To this end, starting from the working principle of each component of a real marine diesel engine system, comprehensive and reasonable thermal performance parameters are chosen to describe their characteristic curves and include them in a one-dimensional thermodynamic model. In particular, the model of a low-speed two stroke MAN 6S50 MC-C8.1 diesel engine is built using the AVL Boost software and obtaining errors lower than 5% between simulated values and test bench data. The behavior of the engine is simulated considering eight multi-fault concomitant phenomena. On this basis, the fault diagnosis method proposed in this paper is verified. The results show that this diagnosis method can effectively isolate the fault propagation phenomenon in the system and quantify the additional irreversibility caused by the Induced factors. The fault diagnosis index proposed in this paper can quickly locate the abnormal components.

Keywords: marine diesel; fault simulation; fault diagnosis; characteristic curve

1. Introduction

Due to the advantages of fuel economy and reliability, diesel engines have attained a leading position in marine applications, and the large two-stroke engine is widely used as the main power plant of civil ships [1,2].

To meet the requirements of Ocean transportation, Marine diesel engine has been developing towards the direction of intelligence and high efficiency [3,4], which also increases the complexity of diesel engine structure. This change increases the possibility of Marine diesel engine system failure. When a failure occurs in a marine main engine system, it will not only produce economic losses but also risk personnel safety

In the past decades, the maintenance of marine diesel engines has evolved from corrective actions to current trends. A lot of studies focus on predictive measures [5] that may improve the reliability of these engines. The purpose of these diagnostic systems is to detect and diagnose diesel engine anomalies before the anomalies cause undesired consequences.

A suitable diagnostic system requires a complete and reliable database that helps identify and diagnose anomalies when symptoms characterizing the abnormality are activated. In order to build a complete and reliable database, diesel engine simulation models have been used to reproduce the fault phenomena [6−8]. With the development of technology, real-time monitoring parameters are becoming more and more comprehensive [9].

In the available historical data on diesel engines, there are usually few historical records of typical faults. Introducing faults in real diesel engines cost a lot of time and fuel, and may compromise the safety of operators and engines [10]. Therefore, it is necessary to build thermodynamic models that act as simulators of the engine to collect faults data [11−13]. The AVLBoost©v2016 software is widely used by the scientific community to construct a one-dimensional wave action model [14−16] by collecting diesel engine geometry and operating data. The validation procedure is then performed by comparing the simulated and experimental values of the main operating parameters, which are obtained either by direct testing or by the manufacturer. On this basis, the virtual platform is constructed to collect the data of the engine under various operating conditions, especially in the case of failure.

A marine diesel engine has a complex structure. When a diesel engine breakdowns, a fault may unstably lead to various symptoms and a detected symptom may be caused by many different faults, which brings considerable difficulties to locate the real root causes of the diesel engine.

In recent years, machine learning and artificial intelligence technology have been widely used in the field of diesel engine fault diagnosis, which provides an effective tool to study the relationship between diesel engine faults and abnormal symptoms [17,18]. The deep learning method can use small data to develop fault diagnosis systems [19,20].

The fault tree method is an effective method to analyze the causal relationship between diesel engine faults and abnormal symptoms, where the diagnosis principle of this method is based on the expert's knowledge of the abnormalities [21,22].

The Marine diesel engine system needs to work in wet, vibratory and other harsh conditions for a long time, which leads to various faults of the Marine diesel engine system during operation. In extreme cases, multiple faults may occur at the same time. When multiple faults occur simultaneously in several different components, the coupling phenomenon between faults will affect the relationship between diesel engine faults and abnormal symptoms.

Therefore, there is a technical problem in the research field of diesel engine fault diagnosis to solve the problem of multi-fault diagnosis [23,24].

With the development of fault diagnosis based on the structural theory of thermoeconomics [25], the useful concepts of "intrinsic" and "induced" malfunctions have emerged [26,27], which may help better understand the causes and effects of failures. Compared with the theory of perturbations [28], the fault diagnosis method based on the thermoeconomic structure theory can obtain more accurate fuel impact values. Valero et al. [29] applied this method to the fault diagnosis of a 160MW coal-fired power plant and analyzed the influence of each component on the fuel consumption of the system. The authors used thermodynamic steady-state simulations to analyze the induced effects (induced malfunction and dysfunction) on other components caused by the intrinsic malfunction of a certain component, and they found that the highest additional fuel plant consumption was attributable to the component where the highest inefficiency occurs.

Verda et al. [30−32] studied the influence of the control system on thermoeconomic diagnosis using simulations to establish the corresponding "free condition" for different operating conditions. This "free condition" was mathematically determined using a specific model of the system. This particular condition is characterized by the same position of the governing parameters as that of the reference condition, but contains the anomalies occurring in the actual operating condition. On this basis, the influence of extra fuel consumption and irreversiblele losses caused by control system intervention is studied. It has been found that the control system intervention may generate higher induced malfunction in some components.

With the deepening of thermal-economic fault diagnosis, researchers [33] found that the complex interaction between components and the intervention of the control system may be the origin of induced malfunctions. These malfunctions are not actual faults within the corresponding components, but they appear because of the mutual interaction between the components' behavior. Thus, the reliability of this fault diagnosis technique may be strongly compromised if the induced malfunction cannot be identified and separated. However, the identification and separation of induced malfunctions are not easy.

Lazzaretto and Stoppato et al. [34] applied this method to the fault diagnosis of multiple complex energy systems to verify the reliability of the method. They found that when the degree of interaction between components in the system is low, this method is effectively able to locate the fault. On the other hand, when the system configuration is complex, this method cannot strictly guarantee the identification of the true source of the fault. The main reason is that it cannot isolate the propagation phenomenon of anomalies, and in turn cannot effectively identify the intrinsic malfunction and induced malfunction, because the variation of an operation parameter generated by the malfunction affects the exergy variables of both the components in which the malfunction occurs and those that suffer an induced malfunction.

On this basis, Toffolo and Lazzaretto et al [35] proposed a new method, named "Characteristic curve method" [36], to detect the malfunctions, based on the idea that the intrinsic malfunction of a component results in a change of its characteristic curve. Therefore, they proposed a new index to check whether the actual operating point of the component moves away from its reference operating condition along the characteristic curve or outside of it. Thus, it can be judged whether the anomaly of the component operation is due to anomalies in other system components (induced malfunctions) or to anomalies within the component (intrinsic malfunction).

In this paper, we propose a diagnosis method based on the characteristic curve of each component

for isolating the propagation phenomena of faults in the system. The goal of this method is to realize the fault location of the diesel engine system When multiple faults occur simultaneously in several different components.

This paper describes the path and mode of fault propagation in the system. Then, based on the characteristics of each component in the diesel engine system, an accurate model of a marine diesel engine system is built after the selection of a suitable set of thermal performance parameters for the accurate description of the characteristic curve of each engine component. The method proposed in this paper is then verified by eight case studies for identifying the failure in the marine diesel engine system.

2. Model

2.1. The engine simulation model

The simulation model of the MAN 6S50 MC-C8.1 Diesel engine was established with AVLBoost©v2020. The specification of the engine are shown in Table 1.

Table 1. Specification of diesel engine.

Parameters	Values
Rated power	9960 kW
Rated speed	127 rpm
Number of cylinders	6
Cylinder bore	500 mm
Stroke	2000 mm
Connecting rod length	2050 mm
Compression ratio	21:1
Turbocharger type	TCA66-21
Bypass valve diameter	61 mm
LHV	4.292×10^7 J/kg
Fire order	1-5-3-4-2-6

According to the manufacturer specifications, the diesel fuel used in the engine certification tests is Marine Gas Oil.

The model simulates the indicated cycle. The gas composition and thermodynamic properties in each element of the intake and exhaust systems piping discretization at any simulation time step (i.e., crank angle) are calculated by solving the one-dimensional conservation equation set commonly used in engine one-dimensional gas-dynamic simulations [37], i.e., mass Eq (1), momentum Eq (2) and energy Eq (3) conservation Eq (4) coupled with the ideal-gas constitutive equation, which writes:

$$\frac{\partial \rho}{\partial t} + \frac{\partial \rho u}{\partial x} = 0 \tag{1}$$

$$\frac{\partial \rho u}{\partial t} + \mu \frac{\partial \rho u}{\partial x} + \frac{\partial p}{\partial x} = 0 \tag{2}$$

$$\frac{\partial(\rho e)}{\partial t}+\left[\frac{\partial(\rho u h)}{\partial x}\right]=0 \tag{3}$$

$$pV = mRT \tag{4}$$

The average cell size is set to 100 (Target Average Cell Size for Spatial Pipe Discretization), and the convergence control is set in several components. The simulation calculation finishes when at least three engine cycles meet the convergence criteria. The convergence criterion is that the variation of the cycle averaged values ("transients") of the IMEP of each cylinder in BOOST™ elements over the last three consecutive cycles is less than a prescribed threshold (500 Pa). In addition, the fuel used in the test bench has the same chemical composition as the vessel.

The components of the model are shown in Figure 1. The system consists of the following components connected by pipes: air filter, compressor, air cooler, intake manifold, cylinders, exhaust manifold and turbine. In the simulation model, measuring points are located in the most relevant positions.

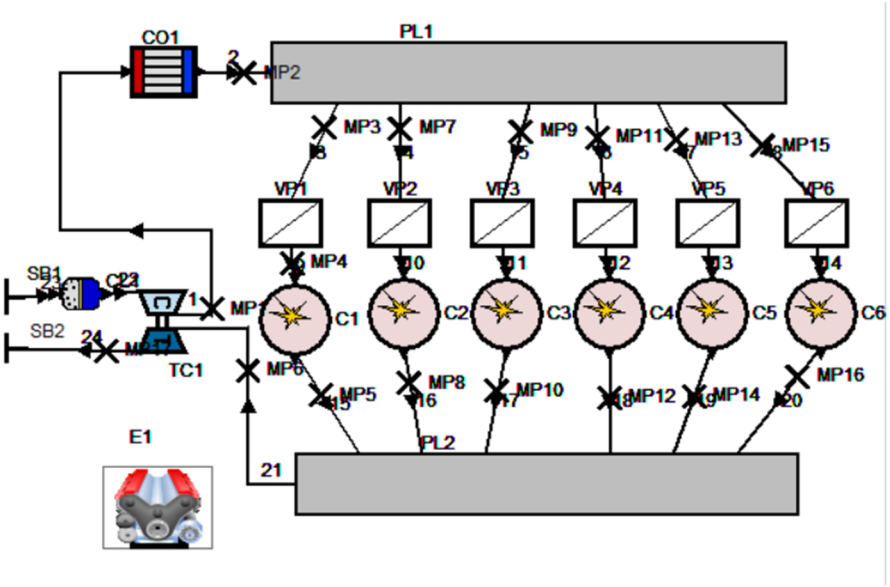

Figure1. The marine diesel engine model AVL BOOST 2020.

The components that make up the model are connected by unidimensional pipes. The pipe parameters include length, equivalent diameter, friction coefficientand wall temperature. The local pressure drop of the air filter is set to a fixed value in the range of 0~0.02 bar. The type of turbocharger is TCA66-21. The complete turbine and compressor maps are input into the marine diesel engine model through tools provided by the software to make sure that the turbocharging process can respond to the actual situation when the boundary conditions change or failure conditions are introduced in the model. The cooling capacity of the air cooler is determined by the inlet temperature of the cooling water and the efficiency of the air cooler. The simulation model considers the actual volume of intake and exhaust manifolds. The heat transfer coefficient of both intake and exhaust manifold models is 0.

Cylinders are defined in terms of their design dimensions, geometric compression ratio, combustion, heat transfer and scavenging port and exhaust valve data. The heat release rate of the combustion process is simulated by a Wiebe law [38−41]. Blow-by is not considered in this article. The lift curve of the scavenging port and exhaust valve is used to determine the filling and emptying

of a cylinder. The Woschni 1990 heat transfer model is used to simulate convective heat losses.

2.2. Model validation

The model was verified by comparing the simulation data with the engine shop test data. Table 2 shows the comparison between the mean values of the simulation and experimental main parameters [42]. The deviation between simulation and experimental values is generally less than 5%. In addition, the verification of the relationship Speed-Power, Speed-SFOC, Speed-Boost Pressure and Speed-Turbocharger Outlet Temperature was also performed, as shown in Figures 2−5.

Therefore, it is considered that the model has good accuracy in simulating engine behavior, and can be used as an abnormal simulation platform without the need to generate failures in a real engine and with a consequent remarkable saving of fuel and time.

Table 2. Comparison between simulated and experimental.

Parameter	100%			75%			50%		
	Measured	Simulated	Error%	Measured	Simulated	Error%	Measured	Simulated	Error%
Power (kW)	9960.00	10236.44	2.78	7470.00	7556.42	1.16	4980.00	5068.86	1.78
Boost Pressure (bar)	4.00	3.94	-1.50	3.15	3.09	-1.84	2.27	2.37	4.24
Compressor Outlet Temperature (K)	475.28	473.60	-0.35	435.72	434.53	-0.27	393.80	390.26	-0.90
Air Mass Flow (kg/s)	25.22	24.76	-1.83	19.69	19.19	-2.54	13.81	13.41	-2.87
Air Cooler Outlet Temperature (K)	310.41	309.80	-0.20	307.64	307.30	-0.11	304.71	304.15	-0.18
P_{max} (bar)	166.90	169.69	1.67	144.70	145.87	0.81	108.30	107.51	-0.73
P_{com} (bar)	146.70	144.03	-1.82	116.00	112.51	-3.01	82.20	84.27	2.52
IMEP (bar)	20.02	20.52	2.50	16.58	16.74	0.97	12.49	12.79	2.40
Turbocharger Inlet Temperature (K)	683.10	688.20	0.75	650.80	657.20	0.98	613.42	599.31	-2.30
Turbocharger Inlet Pressure (bar)	3.75	3.70	-1.33	2.81	2.78	-1.12	2.13	2.21	3.76
Turbocharger Outlet Temperature (K)	526.66	524.80	-0.35	508.1	504.40	-0.73	523.23	514.78	-1.61

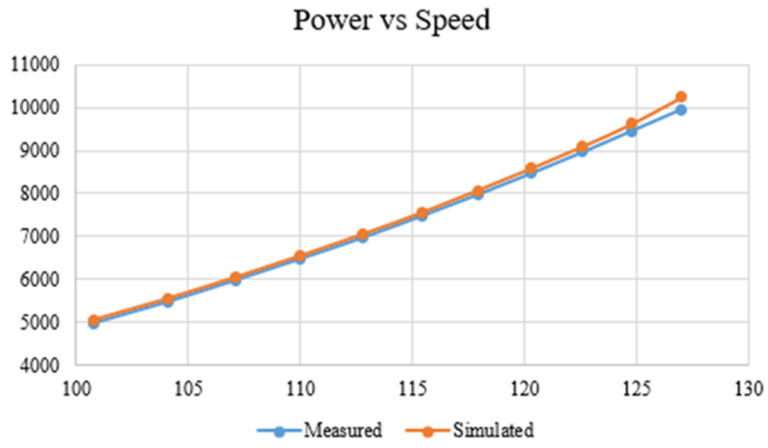

Figure 2. The verification of Speed-Power.

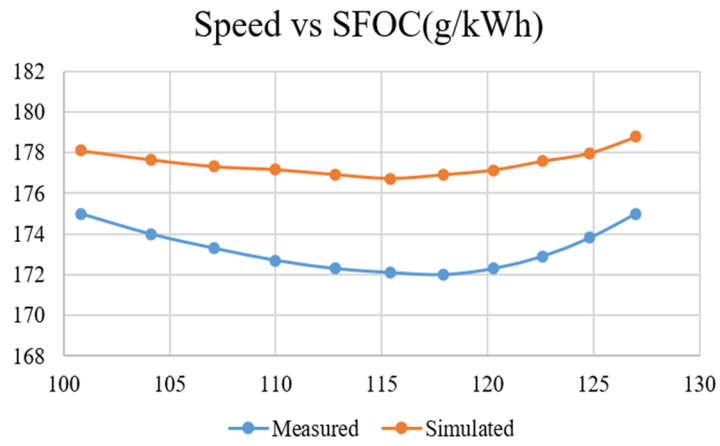

Figure 3. The verification of Speed-SFOC.

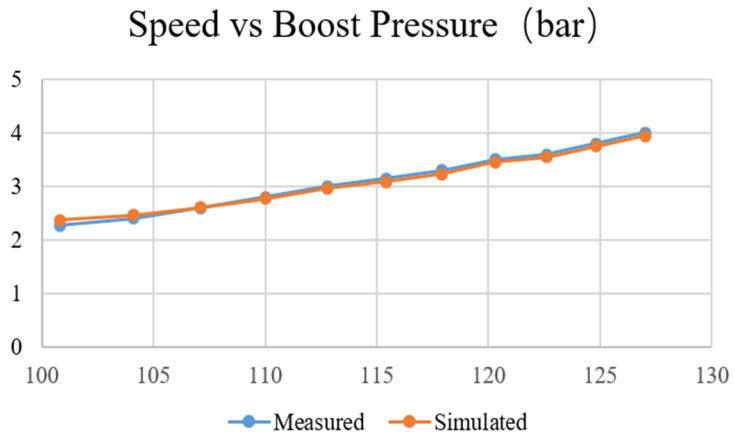

Figure 4. The verification of Speed-Boost Pressure.

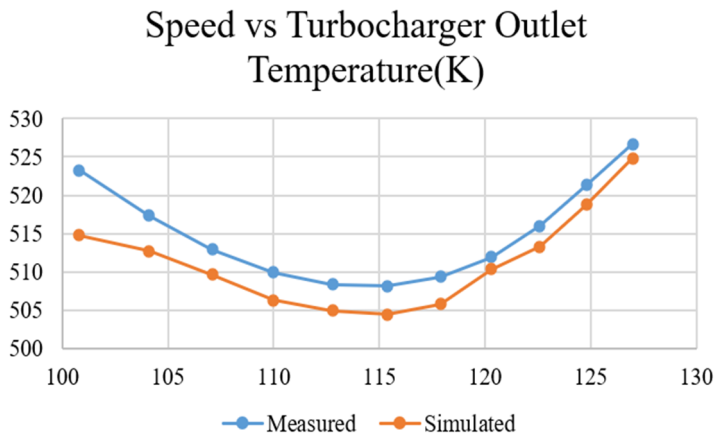

Figure 5. The verification of Speed-Turbocharger Outlet Temperature.

3. Fault location method

3.1. Propagation phenomenon of failure

The mass and energy flow of the diesel engine system is shown in Figure 6. When a component of the system has a failure, the thermodynamic quantities of the mass and energy flow associated with the abnormal component are therefore altered. Due to the interaction among components, this modification affects the operations of other components in turn. Therefore, the impact of the anomaly will propagate through the system, affecting the performance of all relevant components in the system.

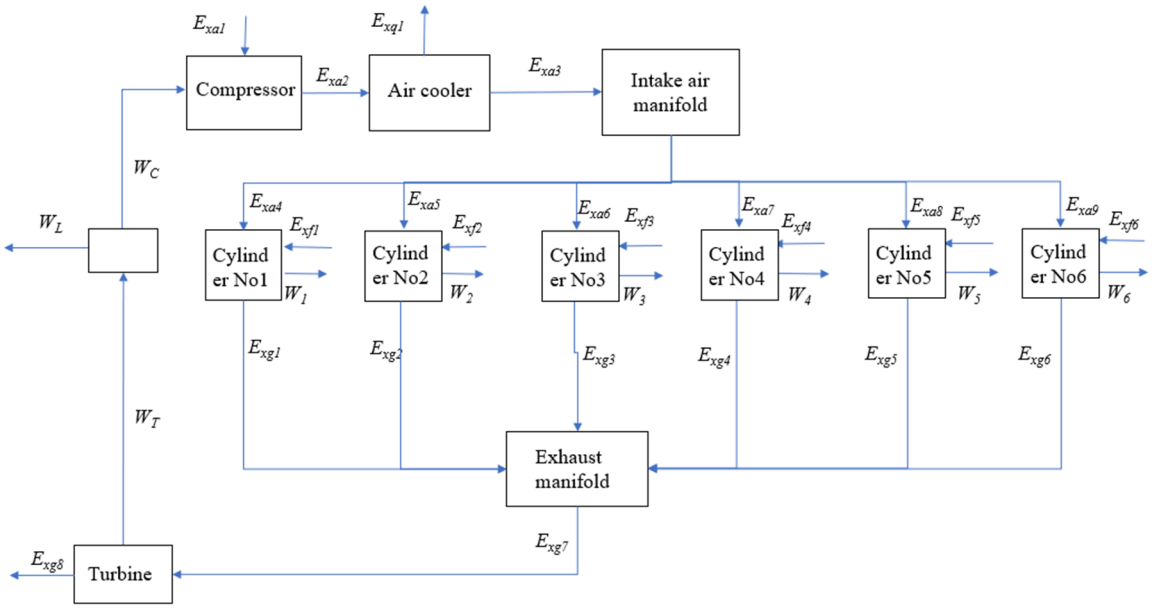

Figure 6. The productive structure diagram.

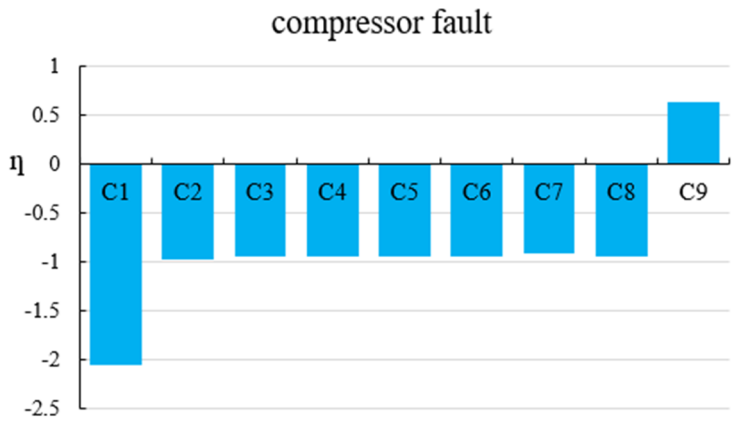

Figure7. Component isentropic efficiency change.

For better and easy understanding, the compressor failure (5% reduction in compressor isentropic efficiency) case is taken as an example. As shown in Figure 7, in the case of a compressor failure, the performance of other components in the system where the anomaly does not exist also changed. This phenomenon occurs because compressor failure changes the operating conditions of other components [36,43]. The failure of the compressor will change the mass flow, pressure and temperature of the air at the outlet of the compressor, resulting in changes in the operating conditions of the air cooler. Although there is no fouling or blockage in the air cooler, the operating state of the air cooler will change accordingly. Based on similar principles, the working performance of components such as cylinders and turbines will also change.

In other words, due to the interaction among components, the changes caused by the intrinsic malfunction can spread throughout the system, creating induced malfunction in the components where the anomaly does not exist. This phenomenon of fault propagation in the system can interfere with fault localization.

3.2. Definition of characteristic curve and diagnostic index

The failure or anomaly of a component (such as changes in the compressor blade geometry, blockage of an air cooler, deposits on heat exchange surfaces, etc.) will affect the functional relationships among the thermodynamic variables (temperature, pressure, mass flow rates, etc.) on which the mass and energy streams involved in the operation of that component depend. These functional relationships are often referred to as component characteristic curves (performance maps in machines, heat transfer models for heat exchangers).

As shown in Figure 8, the operating state of the component will deviate from its original reference state characteristic curve (broken line) and move from the reference state (point A) to a new state (point C). Due to the interaction among components, the alterations caused by the failure of the component will spread through the whole system, affecting the operating states of other components, which react to the changes imposed by the faults in another component according to their non-modified characteristic curves. As shown in Figure 8, the operating state of a component in perfect order will not deviate from the original characteristic curve and move from the reference state (point A) to a new

state (point B). In other words, external factors or induced factors do not affect the characteristic curve of the component that can be affected only by internal factors. External, induced and internal factors are defined as follows [33]: External factors-modification of external conditions such as environment variables. Induced factors-variations caused by the change of other system variables, e.g., component interaction or the intervention of the control system. Internal factors-degradation or failures.

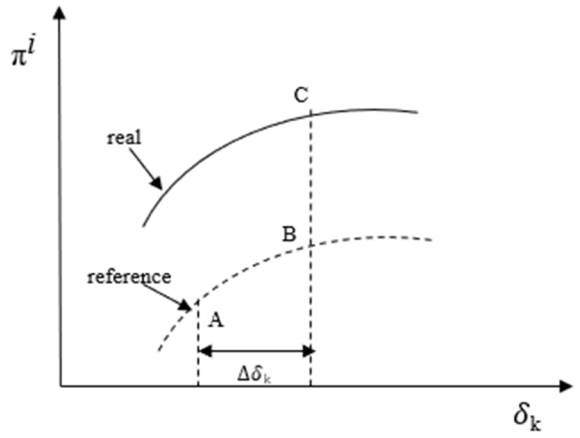

Figure 8. Component operating states.

The location of malfunctioning components depends on the knowledge of the characteristic curve of each component in mathematical form. In particular, Eq (5) formalizes the characteristic curve of the component *i*th by a set of relationships *f* that define a performance parameter or a thermodynamic variable π characterizing the component behavior as a function of a subset δ_k of the independent variables involved in the component operation.

$$\pi^{i,ref}=f^{i,ref}\left(\delta_k^{i,ref}\right) \tag{5}$$

On the other hand, it is always possible to quantify with $\pi^{i,real}$ the actual value of the performance parameter π^i when the component operates at a specific real condition, and with $\mathbf{I}_{index}^i$ the difference between $\pi^{i,real}$ and the value of the performance parameter π^i as expected from Eq (5) for the corresponding operating condition. The difference $\mathbf{I}_{index}^i$ writes as reported in Eq (6).

$$\mathbf{I}_{index}^i=\pi^{i,real}-f^{i,ref}\left(\delta_k^{i,real}\right) \tag{6}$$

Therefore, during the real operation of the component under normal behavior of the system that embeds the component, the result of Eq (6) is zero, since the working point of the component *i*th, corresponds to the operating condition predicted in accordance with the reference characteristic curve. In contrast, when a performance degradation or fault changes the characteristic curve of the component, the result of Eq (6) will be different from zero. Thus, $\mathbf{I}_{index}^i$ can be used as a diagnostic index.

The characteristic curve of the component can be linearly approximated by using its derivative as calculated in the reference state (as shown in Figure 8, the tangent AB_1 in the reference state, approximates the point B with the point B_1, the slope of the tangent AB_1 is the derivative $\partial f^{i,ref}/\partial\delta_k^i$, at

point A, the quantity ε stands for the "residual effects"). In mathematical terms, such approximation can be formalized as reported in Eq (7).

$$f^{ref}\left(\delta_k^{real}\right)-f^{ref}\left(\delta_k^{ref}\right)=\sum_{k=1}^{k}\left[\frac{\partial f^{ref}}{\partial \delta_k}\right]_{\delta_k^{ref}}\left(\delta_k^{real}-\delta_k^{ref}\right) \tag{7}$$

Combining Eq (5) to Eq (7), $\mathbf{I}_{index}^{i}$ can be formulated as

$$\mathbf{I}_{index}^{i}=\pi^{i,real}-\pi^{i,ref}-\left[f^{i,ref}\left(\delta_k^{i,real}\right)-f^{i,ref}\left(\delta_k^{i,ref}\right)\right] \tag{8}$$

$$\mathbf{I}_{index}^{i}=\Delta\pi^{i}-\sum_{k=1}^{k}\left[\frac{\partial f^{i,ref}}{\partial \delta_k}\right]_{\delta_k^{i,ref}}\Delta\delta_k^{i} \tag{9}$$

As shown in Figure 9, if the real operating point of the component is on the original characteristic curve, moving from reference state A to the new state B, the malfunction of the component is only an induced effect. In this case, neglecting the approximation introduced by the linearization of the characteristic curve, $\mathbf{I}_{index}^{i}$= 0. In contrast, if the component has an intrinsic malfunction, the real operating point of the component will depart from the characteristic curve, moving from reference state A to the new state C, and the value of $\mathbf{I}_{index}^{i}$ is expected to be non-zero.

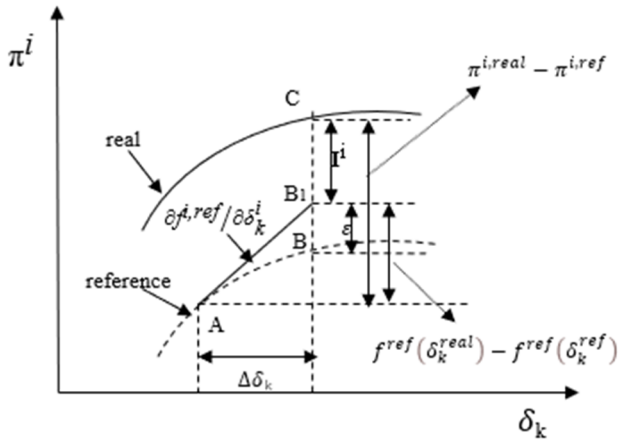

Figure 9. Characteristic curve approximate solution diagram.

3.3. The choice of variable π

The main components in the diesel engine system can be divided into two categories. The first category includes all the "work components", i.e., the components whose product can be expressed as useful exergy. For example, the turbocharger compressor consumes the mechanical work provided by the turbine to increase the internal energy of the air. The second category includes all the "dissipative components", whose product cannot be expressed as useful exergy. For example, the air coolers dissipate heat and reduce the temperature of the cylinder intake air, and the dissipated internal energy is the target product of the air cooler.

In this paper, the irreversibility is selected as parameter π for the diagnostic index $\mathbf{I}_{index}^{i}$ of the components embedded into the diesel engine system. This because:

The irreversibility I^i includes the knowledge related to the mass and energy flows and directly reflects the efficiency of the energy conversion process.

For the "work component", the existence of anomalies will always increase the diagnostic index $\mathbf{I}^i_{index}$.

For the "dissipative component", the existence of anomalies will always reduce the diagnostic index $\mathbf{I}^i_{index}$.

In summary, if the component has an intrinsic malfunction (degradation or failure of the component), the indicator $\mathbf{I}^i_{index}$ of the component will change.

3.4. The characteristic parameters of component

The basic rule for the selection of variables δ^i_k is that they must be a set of independent variables characterizing the behavior of the component. Therefore, the component characteristic curves $f^{i,ref}$, and so the derivatives $\partial f^{i,ref}/\partial\delta^i_k$, can be defined as functions of δ^i_k [36].

For an energy system, all performance variables can be expressed as a function of thermodynamic variables, so thermodynamic variables are the actual independent variables of the energy system.

In addition, exergy represents a synthesis of thermodynamic information that is useful in describing the outcomes of component behavior.

As shown in Section 3.2 of this article, a component's performance is determined by its own physical constraints (characteristic curves) and operational parameters.

Therefore, the natural choice for these variables is a set of independent component thermodynamic variables (including mass flow, pressure and temperature). The number of independent variables is equal to the number of component degrees of freedom.

However, for components with complex production structures or energy conversion, such as cylinders of diesel engines, the required number of independent variables available cannot be monitored. Therefore, specific output parameters should be used to replace the available arguments that cannot be monitored.

As shown in Figure 6, exergy flowing into the compressor includes air exergy flow at compressor inlet E_{xa1} and mechanical exergy W_C.

$$E_{xa1} = f(m_{xa1}, T_{xa1}, P_{xa1}) \tag{10}$$

$$W_C = f(n_C, \boldsymbol{T}_C) \tag{11}$$

Therefore, the independent variable group representing the compressor characteristic curve includes m_{xa1}, T_{xa1}, P_{xa1}, n_C and $\boldsymbol{T}_C$.

However, the signal monitoring of compressor speed and torque is difficult and costly. The relationship between compressor outlet thermal parameters and W_C is shown in Eqs (12)–(15).

$$\eta_C = \frac{(E_{xa2} - E_{xa1})}{W_C} \tag{12}$$

$$\pi = \frac{P_{xa2}}{P_{xa1}} \tag{13}$$

$$T_{xa2} = T_{xa1}\left[1 + \frac{1}{\eta_C}\left(\pi^{\frac{k-1}{k}} - 1\right)\right] \tag{14}$$

$$m_{xa1} = m_{xa2} \tag{15}$$

So, the independent variable group representing the compressor characteristic curve includes m_{xa1}, T_{xa1}, P_{xa1}, T_{xa2} and P_{xa2}.

The selection principle of the independent variable group of the air cooler is similar to the superheater [44]. Considering that the flow rate and pressure of the cooling water are constant. The independent variable group representing the air cooler characteristic curve includes m_{xa2}, T_{xa2}, P_{xa2} and $T_{coolant}$.

For the diesel engine system, the function of the cylinder is to use part of the high-pressure air sent by the compressor to burn the fuel and to mix the combustion products with the rest of the high-pressure air to form high-temperature and high-pressure gas, which drove the piston to produce mechanical exergy as shown in Figure 6. Therefore, the performance of the cylinder is also related to its mechanical structure (design parameters).

Take cylinder No. 1 as an example.

E_{xf1} indicates the chemical exergy of the fuel.

$$E_{xf1} = m_{f1} LHV \tag{16}$$

E_{xa4} represents air exergy flow at the inlet.

$$E_{xa4} = f(m_{xa4}, T_{xa4}, P_{xa4}) \tag{17}$$

E_{xg1} indicates exhaust gas exergy flow.

$$E_{xg1} = f\left(m_{xg1}, T_{xg1}, P_{xg1}\right) \tag{18}$$

Thermodynamic processes, chemical reactions, mechanical work, heat transfer, mass diffusion and friction processes occur simultaneously within this component. In other words, the irreversible losses in the working process of the cylinder must include irreversibility losses due to fuel combustion, cylinder heat transfer, exhaust gas, mechanical friction, etc. The description of each irreversibility loss requires monitoring a large number of characteristic parameters, such as compression end temperature, atomization of the fuel in the cylinder, etc., which are very demanding to be managed and some of the parameters are not easy to measure with the standard marine engine technology. On the other hand, the overall irreversibility loss in the cylinder can be calculated by the cylinder input energy and the cylinder output work.

The indicated mean effective pressure (IMEP) is the work output of one cycle for unit swept volume and relates to the cylinder power in accordance with Eq (19).

$$W_i = \frac{n}{60} IMEP_i\left(\frac{\pi S D^2}{4}\right) \tag{19}$$

W_i——Power of the ith cylinder, [kW]

n——diesel engine speed, [r/min]

$IMEP_i$——Mean Effective Pressure of the ith cylinder, [kPa]

D——bore, [mm]
S——stroke, [mm]

Therefore, for the diesel engine system, the independent variable group representing the cylinder No. 1 characteristic curve includes m_{xa4}, T_{xa4}, P_{xa4}, and m_{f1}.

The selection principle of the independent variable group of the turbine is similar to the compressor. However, according to the differences between the compressor map and the turbine map, the independent variable group representing the turbine characteristic curve includes m_{xa7}, T_{xa7}, P_{xa7} and P_{xa8}.

The characteristic parameters selected for the cylinder and all of the other engine components considered in this study are shown in Tables 3 to 6. It should be noted that the fuel quantity injected in each cylinder is assumed here as a constant value related to the diesel engine load because, in current diesel engine systems, it is difficult to monitor the flow rate in each fuel injector.

The measurement points setting in the simulation model are shown in Figure 10.

Table 3. Characteristic parameters of the compressor.

p_{MP1}	Compressor inlet air pressure (bar)
p_{MP2}	Compressor outlet air pressure (bar)
m_{MP1}	Compressor outlet air mass flow rate (kg/s)
T_{MP1}	Compressor inlet air temperature (K)
T_{MP2}	Compressor outlet air temperature (K)

Table 4. Characteristic parameters of the air cooler.

T_{MP2}	Compressor outlet air temperature (K)
$T_{coolant}$	Air cooler outlet air temperature (K)
p_{MP2}	Compressor outlet air pressure (bar)
m_{MP2}	Air cooler inlet air mass flow rate (kg/s)

Table 5. Characteristic parameters of the cylinder.

$m_{MP4\sim9}$	Cylinder intake air mass flow rate (kg/s)
p_{MP3}	Cylinder intake air pressure (bar)
T_{MP3}	Cylinder intake air temperature (K)
$m_{fuel\ MP4\sim9}$	Fuel mass flow rate (g/s)

Table 6. Characteristic parameters of the turbine.

P_{MP10}	Turbine inlet gas pressure (bar)
T_{MP10}	Turbine inlet gas temperature (K)
p_{MP11}	Turbine outlet gas pressure (bar)
m_{MP10}	Turbine inlet gas mass flow rate (kg/s)

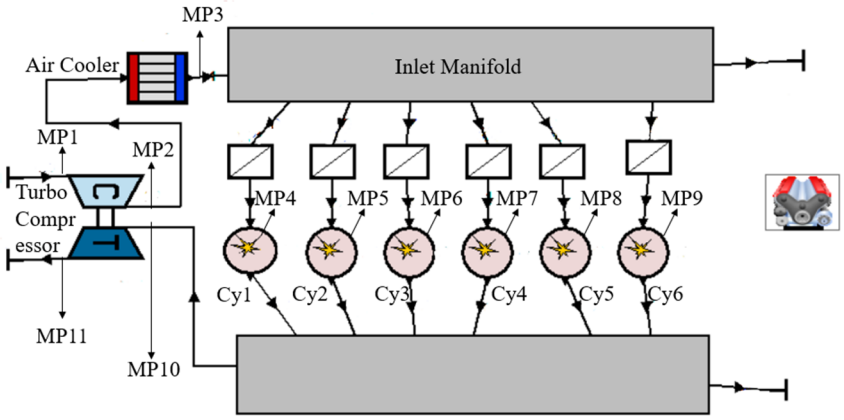

Figure 10. measurement points setting.

3.5. The fault indicator

For "work components" the diagnostic index $\mathbf{I}^{i}_{index}$ can be expressed as in Eq (20).

$$\mathbf{I}^{i}_{index}=\Delta I^{i}-\Delta I^{i,calc}=I^{i,real}-\sum_{k}\left[\frac{\partial I^{i,ref}}{\partial \delta^{i}_{k}}\right]_{\delta^{i,ref}_{k}}\Delta\delta^{i}_{k} \tag{20}$$

For "dissipative components" the diagnostic index $\mathbf{I}^{i}_{index}$ can be expressed in Eq (21).

$$\mathbf{I}^{i}_{index}=-\left(\Delta I^{i}-\Delta I^{i,calc}\right)=\sum_{k}\left[\frac{\partial I^{i,ref}}{\partial \delta^{i}_{k}}\right]_{\delta^{i,ref}_{k}}\Delta\delta^{i}_{k}-I^{i,real} \tag{21}$$

The $\Delta I^{i,calc}$ is the expected variation of component irreversibility due to a change $\Delta\delta k$ of the component independent variables, according to the reference component characteristic curve.

Since the analytic form of each characteristic curve is generally unknown, the derivatives $\partial I^{i,ref}/\partial\delta^{i}_{k}$ of every component can be calculated by generating several virtual operating conditions near the reference operation using a simulator.

In order to make the reference state close to the actual state, it is necessary to change the diesel engine speed and fuel injection quantity.

$$\mathrm{n}=n_{e}\left(\frac{W}{W_{e}}\right)^{1/3} \tag{22}$$

W_e——Nominal engine power, [kW]
n_e——Nominal engine speed, [r/min]
W——Diesel engine power, [kW]
n——Diesel engine speed, [r/min]

$$\Delta h=\frac{100g_{e}W}{60\gamma Ln} \tag{23}$$

Δh——The amount of oil supplied to one cylinder in 100 engine cycles, [ml];

g_e——Fuel consumption rate, [g/(kW·h)];
W——Diesel engine power, [kW];
γ——Density of fuel oil, 0.825[g/(cm3)] for diesel;
L——Number of cylinders;
n——Diesel engine speed, [rpm].

In the reference state, Eq (22) allows calculating the speed of the diesel engine, whereas Eq (23) allows estimating the amount of fuel injected in the cylinder.

Taking the turbine as an example, four virtual operating conditions (ref1, ref2, ref3 and ref4) are required to calculate the derivatives of the turbine, since the number of component independent variables is four (P_{MP10}, T_{MP10}, P_{MP11} and m_{MP10}). as shown in Eq (24). Note that the turbine outlet pressure is an environmental variable (atmospheric pressure). To avoid the rank of the equations being less than the number of independent variables of the equation, resulting in countless solutions to the equation, at least two different turbine outlet pressures should be set among the four reference states generated by the simulation simulator.

$$\begin{bmatrix} \Delta^{ref1}T_{MP10} & \Delta^{ref1}P_{MP10} & \Delta^{ref1}m_{MP10} & \Delta^{ref1}P_{MP11} \\ \Delta^{ref2}T_{MP10} & \Delta^{ref2}P_{MP10} & \Delta^{ref2}m_{MP10} & \Delta^{ref2}P_{MP11} \\ \Delta^{ref3}T_{MP10} & \Delta^{ref3}P_{MP10} & \Delta^{ref3}m_{MP10} & \Delta^{ref3}P_{MP11} \\ \Delta^{ref4}T_{MP10} & \Delta^{ref4}P_{MP10} & \Delta^{ref4}m_{MP10} & \Delta^{ref4}P_{MP11} \end{bmatrix} \begin{bmatrix} \partial I/\partial T_{MP10} \\ \partial I/\partial P_{MP10} \\ \partial I/\partial m_{MP10} \\ \partial I/\partial P_{MP11} \end{bmatrix} = \begin{bmatrix} \Delta^{ref1}I \\ \Delta^{ref2}I \\ \Delta^{ref3}I \\ \Delta^{ref4}I \end{bmatrix} \tag{24}$$

4. Results and discussion

Once the model has been adjusted and validated, failures are introduced one by one.

The compressor failure F1 is usually caused by dust accumulation in the impeller or diffuser as well as damages that produce changes in geometry. The compressor failure is simulated by reducing the isentropic efficiency of the compressor.

The air cooler failure F2 is usually caused by the increase of fouling on the inner wall of the air cooler, which will produce a reduction of cooling capacity. The air cooler failure is simulated by reducing the isentropic efficiency.

This kind of cylinder failure F3 (Blocking of the injector hole of the cylinder) is usually caused by the fault of the fuel injection system or the carbon accumulation of the nozzle, resulting in a reduction in the corresponding fuel mass flow rate.

This kind of cylinder failure F4 (Excessive blow-by) is usually caused by abnormal wear of the piston ring, which is simulated by increasing the clearance between the piston ring and the sleeve.

The turbine failure F5 is usually caused by dust accumulation in the impeller or diffuser as well as damages that produce changes in geometry. The turbine failure is simulated by reducing the isentropic efficiency of the turbine.

In this paper, the method has been verified by cases real 1~8 as shown in Table 7.

Table 8 provides the details of cases real 1 to real 8.

Table 9 provides the details of the of the reference cases.

Table 7. Cases real 1−8.

	F1	F2	F3	F4	F5
Real 1	a 5% reduction in compressor efficiency	a 10% decrease in air cooler efficiency			
Real 2	a 5% reduction in compressor efficiency		Cylinder No 1 a 10% reduction in fuel mass flow rate		
Real 3	a 5% reduction in compressor efficiency				a 10% reduction in turbine efficiency
Real 4		a 10% decrease in air cooler efficiency	Cylinder No 1 a 10% reduction in fuel mass flow rate		
Real 5		a 10% decrease in air cooler efficiency			a 10% reduction in turbine efficiency
Real 6			Cylinder No 1 a 10% reduction in fuel mass flow rate		a 10% reduction in turbine efficiency
Real 7			Cylinder No 2 a 6% reduction in fuel mass flow rate	Cylinder No 1 a 0.03mm increase in the gap	
Real 8	a 5% reduction in compressor efficiency	a 5% decrease in air cooler efficiency	Cylinder No 1 a 4% reduction in fuel mass flow rate		a 5% reduction in turbine efficiency

Table 8. Operating conditions of the test cases real 1−8.

Component		real 1	real 2	real 3	real 4	real 5	real 6	real 7	real 8
Component	Power	10101.59	10008.32	9870.52	10031.25	9972.35	9870.52	10011.61	9949.40
	Speed	127.00	127.00	127.00	127.00	127.00	127.00	127.00	127.00
Compressor	p_{MP1} (bar)	1.00	1.00	1.00	1.00	1.00	1.00	1.00	1.00
	T_{MP1} (k)	298.00	298.00	298.00	298.00	298.00	298.00	298.00	298.00
	p_{MP2} (bar)	3.8762	3.7971	3.5471	3.9688	3.7377	3.5471	3.8825	3.7097
	T_{MP2} (k)	477.4590	474.0320	460.9100	475.5320	461.4190	460.9100	471.6820	468.8950
	m_{MP1} (kg/s)	24.0140	23.6731	21.6248	24.7353	22.8813	21.6248	24.4767	22.8091
	I (kW)	590.2936	588.1848	484.5482	543.8361	417.8556	484.5482	527.8811	538.8710
Air cooler	p_{MP2} (bar)	3.8762	3.7971	3.5471	3.9688	3.7377	3.5471	3.8825	3.7097
	T_{MP2} (k)	477.4590	474.0320	460.9100	475.5320	461.4190	460.9100	471.6820	468.8950
	m_{MP2} (kg/s)	24.0140	23.6731	21.6248	24.7353	22.8813	21.6248	24.4767	22.8091
	$T_{coolant}$ (k)	300.9628	301.2222	300.7220	301.0291	300.5774	300.7220	301.2871	300.8501
	I (kW)	916.5564	891.4642	714.6946	925.5231	743.2062	714.6946	900.3024	812.0430

Continued on next page

Component		Real 1	Real 2	Real 3	Real 4	Real 5	Real 6	Real 7	Real 8
Cylinder No.1	m_{MP4} (kg/s)	3.9903	4.0157	3.6091	4.2625	3.8190	3.6101	4.1066	3.8595
	T_{MP3} (k)	328.2280	309.8090	308.9140	327.8810	325.4980	308.9140	309.6450	318.0570
	p_{MP3} (bar)	3.8539	3.7764	3.5285	3.9456	3.7166	3.5285	3.8608	3.6743
	$m_{fuelMP4}$(g/s)	84.7281	84.7281	84.7281	84.7281	84.7281	84.7281	84.7281	84.7281
	I (kW)	1609.2403	1809.7893	1677.1512	1777.9652	1636.7783	1819.7841	1725.5175	1695.2112
Cylinder No.2	m_{MP5}(kg/s)	3.9904	3.9424	3.6106	4.1023	3.8195	3.6106	4.1021	3.7836
	T_{MP3} (k)	328.2280	309.8090	308.9140	327.8810	325.4980	308.9140	309.6450	318.0570
	p_{MP3} (bar)	3.8539	3.7764	3.5285	3.9456	3.7166	3.5285	3.8608	3.6743
	$m_{fuelMP5}$(g/s)	84.7281	84.7281	84.7281	84.7281	84.7281	84.7281	84.7281	84.7281
	I (kW)	1609.2929	1624.2397	1677.9318	1599.3272	1636.6314	1661.6587	1727.9578	1647.2573
Cylinder No.3	m_{MP6}(kg/s)	3.9902	3.9438	3.6097	4.0937	3.8186	3.6097	4.0489	3.7886
	T_{MP3} (k)	328.2280	309.8090	308.9140	327.8810	325.4980	308.9140	309.6450	318.0570
	p_{MP3} (bar)	3.8539	3.7764	3.5285	3.9456	3.7166	3.5285	3.8608	3.6743
	$m_{fuelMP6}$(g/s)	84.7281	84.7281	84.7281	84.7281	84.7281	84.7281	84.7281	84.7281
	I (kW)	1609.4291	1624.4081	1677.2958	1599.6861	1636.7783	1661.1583	1617.4147	1647.9721
Cylinder No.4	m_{MP7}(kg/s)	3.9910	3.9415	3.6110	4.0957	3.8199	3.6110	4.0453	3.7866
	T_{MP3} (k)	328.2280	309.8090	308.9140	327.8810	325.4980	308.9140	309.6450	318.0570
	p_{MP3} (bar)	3.8539	3.7764	3.5285	3.9456	3.7166	3.5285	3.8608	3.6743
	$m_{fuelMP7}$(g/s)	84.7281	84.7281	84.7281	84.7281	84.7281	84.7281	84.7281	84.7281
	I (kW)	1609.0834	1623.8874	1677.4387	1599.9480	1636.4972	1661.7664	1618.2848	1647.6579
Cylinder No.5	m_{MP8}(kg/s)	3.9910	3.9419	3.6108	4.1041	3.8196	3.6108	4.0462	3.7884
	T_{MP3} (k)	328.2280	309.8090	308.9140	327.8810	325.4980	308.9140	309.6450	318.0570
	p_{MP3} (bar)	3.8539	3.7764	3.5285	3.9456	3.7166	3.5285	3.8608	3.6743
	$m_{fuelMP8}$(g/s)	84.7281	84.7281	84.7281	84.7281	84.7281	84.7281	84.7281	84.7281
	I (kW)	1608.6447	1623.9011	1677.5424	1599.2707	1636.4317	1661.3591	1617.5661	1647.2000
Cylinder No.6	m_{MP9}(kg/s)	3.9911	3.9547	3.6113	4.1042	3.8201	3.6113	4.0481	3.7930
	T_{MP3} (k)	328.2280	309.8090	308.9140	327.8810	325.4980	308.9140	309.6450	318.0570
	p_{MP3} (bar)	3.8539	3.7764	3.5285	3.9456	3.7166	3.5285	3.8608	3.6743
	$m_{fuelMP9}$(g/s)	84.7281	84.7281	84.7281	84.7281	84.7281	84.7281	84.7281	84.7281
	I (kW)	1609.0873	1623.5847	1677.6551	1599.5612	1636.4519	1661.9530	1617.3856	1647.1802
Turbine	T_{MP10} (k)	708.7570	694.6990	724.6460	692.9160	718.5590	724.6460	686.3560	713.3450
	p_{MP10} (bar)	3.6509	3.5806	3.3529	3.7336	3.5244	3.3529	3.6572	3.4997
	p_{MP11} (bar)	1.00	1.00	1.00	1.00	1.00	1.00	1.00	1.00
	m_{MP10} (kg/s)	24.4572	24.2325	22.1887	25.3028	23.4416	22.1887	24.9044	23.3626
	I (kW)	1007.7137	947.5502	996.5011	1040.8258	1120.6941	996.5011	983.9835	999.5440

Table 9. Operating conditions of the reference cases.

Component		Reference 1	Reference 2/7	Reference 3/6	Reference 4	Reference 5	Reference 8
	Power	10121.74	10000.04	9847.98	10032.55	9972.65	9938.45
	Speed	126.53	126.03	125.39	126.16	125.90	125.78
Compressor	p_{MP1} (bar)	1.00	1.00	1.00	1.00	1.00	1.00
	T_{MP1} (k)	298.00	298.00	298.00	298.00	298.00	298.00
	p_{MP2} (bar)	472.8810	471.9370	470.9190	472.2240	471.7400	471.4240
	T_{MP2} (k)	3.9128	3.8927	3.8714	3.8986	3.8889	3.8826
	m_{MP1} (kg/s)	24.5439	24.4783	24.3974	24.4960	24.4661	24.4456
	I (kW)	529.6744	524.8292	519.2297	526.3677	523.6595	521.8509
Air cooler	p_{MP2} (bar)	472.8810	471.9370	470.9190	472.2240	471.7400	471.4240
	T_{MP2} (k)	3.9128	3.8927	3.8714	3.8986	3.8889	3.8826
	m_{MP2} (kg/s)	24.5439	24.4783	24.3974	24.4960	24.4661	24.4456
	$T_{coolant}$ (k)	301.3312	301.3177	301.3044	301.3221	301.3158	301.3101
	I (kW)	913.2281	902.2365	890.1123	905.4889	900.0049	896.4213
Cylinder No.1	m_{MP4} (kg/s)	4.1023	4.0896	4.0758	4.0938	4.0871	4.0842
	T_{MP3} (k)	309.7140	309.6520	309.5720	309.6690	309.6370	309.6170
	p_{MP3} (bar)	3.8912	3.8710	3.8498	3.8770	3.8673	3.8610
	$m_{fuelMP4}$ (g/s)	83.6891	82.6337	81.2945	82.9081	82.3911	82.0924
	I (kW)	1594.1865	1573.4135	1557.0461	1578.7562	1568.7056	1562.6779
Cylinder No.2	m_{MP5} (kg/s)	4.1037	4.0905	4.0781	4.0948	4.0877	4.0846
	T_{MP3} (k)	309.7140	309.6520	309.5720	309.6690	309.6370	309.6170
	p_{MP3} (bar)	3.8912	3.8710	3.8498	3.8770	3.8673	3.8610
	$m_{fuelMP5}$ (g/s)	83.6891	82.6337	81.2945	82.9081	82.3911	82.0924
	I (kW)	1594.3725	1573.7743	1557.4783	1579.1466	1569.0888	1563.0352
Cylinder No.3	m_{MP6} (kg/s)	4.1034	4.0911	4.0780	4.0952	4.0886	4.0858
	T_{MP3} (k)	309.7140	309.6520	309.5720	309.6690	309.6370	309.6170
	p_{MP3} (bar)	3.8912	3.8710	3.8498	3.8770	3.8673	3.8610
	$m_{fuelMP6}$ (g/s)	83.6891	82.6337	81.2945	82.9081	82.3911	82.0924
	I (kW)	1594.4340	1573.7983	1557.3504	1579.1632	1569.1054	1563.0620
Cylinder No.4	m_{MP7} (kg/s)	4.1028	4.0910	4.0781	4.0950	4.0885	4.0858
	T_{MP3} (k)	309.7140	309.6520	309.5720	309.6690	309.6370	309.6170
	p_{MP3} (bar)	3.8912	3.8710	3.8498	3.8770	3.8673	3.8610
	$m_{fuelMP7}$ (g/s)	83.6891	82.6337	81.2945	82.9081	82.3911	82.0924
	I (kW)	1594.1327	1573.7921	1557.7090	1579.1570	1569.1009	1563.0571
Cylinder No.5	m_{MP8} (kg/s)	4.1024	4.0901	4.0785	4.0941	4.0875	4.0849
	T_{MP3} (k)	309.7140	309.6520	309.5720	309.6690	309.6370	309.6170
	p_{MP3} (bar)	3.8912	3.8710	3.8498	3.8770	3.8673	3.8610
	$m_{fuelMP8}$ (g/s)	83.6891	82.6337	81.2945	82.9081	82.3911	82.0924
	I (kW)	1594.0624	1573.7699	1557.6131	1579.1352	1569.0844	1563.0397

Continued on next page

Component		Reference 1	Reference 2/7	Reference 3/6	Reference 4	Reference 5	Reference 7
Cylinder No.6	m_{MP9} (kg/s)	4.1030	4.0912	4.0784	4.0951	4.0889	4.0862
	T_{MP3} (k)	309.7140	309.6520	309.5720	309.6690	309.6370	309.6170
	p_{MP3} (bar)	3.8912	3.8710	3.8498	3.8770	3.8673	3.8610
	$m_{fuelMP9}$ (g/s)	83.6891	82.6337	81.2945	82.9081	82.3911	82.0924
	I (kW)	1594.0157	1573.6686	1557.9887	1579.0240	1568.9687	1562.9689
Turbine	T_{MP10} (k)	684.4270	681.5690	677.4410	682.2210	680.8030	680.0880
	p_{MP10} (bar)	3.6873	3.6674	3.6462	3.6732	3.6636	3.6575
	p_{MP11} (bar)	1.00	1.00	1.00	1.00	1.00	1.00
	m_{MP10} (kg/s)	25.1447	25.0634	24.9964	25.0908	25.0521	25.0236
	I (kW)	1000.8812	984.6433	965.2654	989.1949	981.1677	976.3621

Table 10. The diagnosis results of case real 1.

Component	$I^{i,\text{real}}$ (kW)	$I^{i,\text{ref}}$ (kW)	ΔI^{i} (kW)	$\Delta I^{i,calc}$ (kW)	$\mathbf{I}^{i}_{index}$ (kW)	$\mathbf{I}^{i}_{index}/\lvert\Delta I^{i,calc}\rvert$%
Compressor	**590.2936**	**529.6744**	**60.6192**	**21.8848**	**38.7344**	**176.9926**
Air cooler	**916.5564**	**913.2281**	**3.3284**	**24.0278**	**20.6995**	**86.1478**
Cy 1	1609.2403	1594.1865	15.0538	14.8395	0.2142	1.4437
Cy 2	1609.2929	1594.3725	14.9204	15.0179	-0.0974	-0.6489
Cy 3	1609.4291	1594.4340	14.9951	15.3693	-0.3743	-2.4353
Cy 4	1609.0834	1594.1327	14.9507	14.9858	-0.0352	-0.2348
Cy 5	1608.6447	1594.0624	14.5823	14.9877	-0.4054	-2.7047
Cy 6	1609.0873	1594.0157	15.0715	15.2218	-0.1502	-0.9870
Turbine	1007.7137	1000.8812	6.8326	6.7613	0.0713	1.0550

Table 11. The diagnosis results of case real 2.

Component	$I^{i,\text{real}}$ (kW)	$I^{i,\text{ref}}$ (kW)	ΔI^{i} (kW)	$\Delta I^{i,calc}$ (kW)	$\mathbf{I}^{i}_{index}$ (kW)	$\mathbf{I}^{i}_{index}/\lvert\Delta I^{i,calc}\rvert$%
Compressor	**588.1848**	**524.8292**	**63.3556**	**49.4634**	**13.8922**	**28.0859**
Air cooler	891.4642	902.2365	-10.7722	-10.5130	0.2593	-2.4663
Cy 1	**1809.7893**	**1573.4135**	**236.3758**	**39.0900**	**197.2858**	**504.6960**
Cy 2	1624.2397	1573.7743	50.4654	48.7256	1.7399	3.5708
Cy 3	1624.4081	1573.7983	50.6098	48.9432	1.6666	3.4052
Cy 4	1623.8874	1573.7921	50.0953	48.4611	1.6342	3.3722
Cy 5	1623.9011	1573.7699	50.1312	48.4779	1.6533	3.4105
Cy 6	1622.1847	1573.6686	49.9160	48.7887	1.1274	2.4095
Turbine	947.5502	984.6433	-37.0930	-36.0665	-1.0265	-2.8462

Table 12. The diagnosis results of case real 3.

Component	$I^{i,\text{real}}$ (kW)	$I^{i,\text{ref}}$ (kW)	ΔI^{i} (kW)	$\Delta I^{i,calc}$ (kW)	$\mathbf{I}^{i}_{index}$ (kW)	$\mathbf{I}^{i}_{index}/\lvert\Delta I^{i,calc}\rvert$%
Compressor	**484.5482**	**519.2297**	**-34.6815**	**-57.4066**	**22.7251**	**39.5863**
Air cooler	714.6946	890.1193	-177.6476	-179.8806	-2.2330	-1.2414
Cy 1	1677.1512	1557.0461	120.1052	118.6846	1.4206	1.1969
Cy 2	1677.9318	1557.4783	120.4536	119.6224	0.8311	0.6948
Cy 3	1677.2958	1557.3504	119.9454	117.0232	2.9222	2.4971
Cy 4	1677.4387	1557.7090	119.7297	117.9290	1.8007	1.5269
Cy 5	1677.5424	1557.6131	119.9294	118.0559	1.8735	1.5869
Cy 6	1677.6551	1557.9887	119.6663	118.1203	1.5461	1.3089
Turbine	**996.5011**	**965.2654**	**31.2358**	**-154.0653**	**185.3011**	**120.2744**

Table 13. The diagnosis results of case real 4.

Component	$I^{i,\text{real}}$ (kW)	$I^{i,\text{ref}}$ (kW)	ΔI^{i} (kW)	$\Delta I^{i,calc}$ (kW)	$\mathbf{I}^{i}_{index}$ (kW)	$\mathbf{I}^{i}_{index}/\lvert\Delta I^{i,calc}\rvert$%
Compressor	543.8361	526.3677	17.4684	17.7287	-0.2603	-1.4684
Air cooler	**925.5231**	**905.4889**	**20.0342**	**43.1923**	**23.1581**	**53.6163**
Cy 1	**1777.9652**	**1578.7562**	**199.2090**	**35.5401**	**163.6689**	**460.5190**
Cy 2	1599.3272	1579.1466	20.1806	19.9047	0.2759	1.3862
Cy 3	1599.6861	1579.1632	20.5229	21.1479	-0.6250	-2.9554
Cy 4	1599.9480	1579.1570	20.7910	21.1904	-0.3995	-1.8851
Cy 5	1599.2707	1579.1352	20.1354	20.7289	-0.5934	-2.7310
Cy 6	1599.5612	1579.0240	20.5372	20.9748	-0.4376	-2.0863
Turbine	1040.8258	989.1949	51.6309	52.6778	-1.0469	-1.9873

Table 14. The diagnosis results of case real 5.

Component	$I^{i,\text{real}}$ (kW)	$I^{i,\text{ref}}$ (kW)	ΔI^{i} (kW)	$\Delta I^{i,calc}$ (kW)	$\mathbf{I}^{i}_{index}$ (kW)	$\mathbf{I}^{i}_{index}/\lvert\Delta I^{i,calc}\rvert$%
Compressor	417.8556	523.6595	-105.8039	-103.0259	-2.7780	-2.6964
Air cooler	**743.2062**	**900.0049**	**-156.7987**	**-131.5464**	**25.2523**	**19.1965**
Cy 1	1636.7783	1568.7056	67.6568	68.0104	-0.3536	-0.5199
Cy 2	1636.6314	1569.0888	67.5426	68.1260	-0.5834	-0.8563
Cy 3	1636.7783	1569.1054	67.6729	69.8527	-2.1799	-3.1206
Cy 4	1636.4972	1569.1009	67.3964	67.7826	-0.3863	-0.5698
Cy 5	1636.4317	1569.0844	67.3473	67.8048	-0.4576	-0.6748
Cy 6	1636.4519	1568.9687	67.4832	67.7599	-0.2767	-0.4083
Turbine	**1120.6941**	**981.1677**	**139.5264**	**-35.4264**	**174.9529**	**493.8486**

Table 15. The diagnosis results of case real 6.

Component	$I^{i,\text{real}}$ (kW)	$I^{i,\text{ref}}$ (kW)	ΔI^{i} (kW)	$\Delta I^{i,calc}$ (kW)	$\mathbf{I}^{i}_{index}$ (kW)	$\mathbf{I}^{i}_{index}/\lvert\Delta I^{i,calc}\rvert$%
Compressor	407.3916	519.2297	-111.8381	-114.0352	2.1970	1.9266
Air cooler	721.9432	890.1123	-168.1691	-164.7713	3.3979	2.0622
Cy 1	**1819.7841**	1557.0461	**262.7380**	**92.4313**	**170.3067**	**184.2522**
Cy 2	1661.6587	1557.4783	104.6645	104.2440	0.4205	0.4034
Cy 3	1661.1583	1557.3504	103.8179	103.9990	-0.1810	-0.1741
Cy 4	1661.7664	1557.7090	104.0574	103.9191	0.1384	0.1331
Cy 5	1661.3591	1557.6131	103.7461	103.9487	-0.2026	-0.1949
Cy 6	1661.9530	1557.9887	103.9643	103.2496	0.7147	0.6922
Turbine	**1051.9641**	**965.2654**	**86.6987**	**-104.1079**	**190.8067**	**183.2777**

Table 16. The diagnosis results of case real 7.

Component	$I^{i,\text{real}}$ (kW)	$I^{i,\text{ref}}$ (kW)	ΔI^{i} (kW)	$\Delta I^{i,calc}$ (kW)	$\mathbf{I}^{i}_{index}$ (kW)	$\mathbf{I}^{i}_{index}/\lvert\Delta I^{i,calc}\rvert$%
Compressor	527.8811	529.6744	-1.7933	-1.7847	-0.0085	-0.4788
Air cooler	900.3024	913.2281	-12.9257	-13.0193	0.0936	-0.7188
Cy 1	**1725.5175**	**1573.4135**	**152.1040**	**36.2904**	**115.8136**	**319.1300**
Cy 2	**1727.9578**	**1573.7743**	**154.1836**	**36.4593**	**117.7242**	**322.8919**
Cy 3	1617.4147	1573.7983	43.6164	44.3608	-0.7444	-1.6780
Cy 4	1618.2848	1573.7921	44.4928	44.5381	-0.0454	-0.1018
Cy 5	1617.5661	1573.7699	43.7963	44.3335	-0.5373	-1.2119
Cy 6	1617.3856	1573.6686	43.7170	44.0129	-0.2960	-0.6725
Turbine	983.9835	1000.8812	-16.8977	-16.4867	-0.4110	-2.4929

Table 17. The diagnosis results of case real 8.

Component	$I^{i,\text{real}}$ (kW)	$I^{i,\text{ref}}$ (kW)	ΔI^{i} (kW)	$\Delta I^{i,calc}$ (kW)	$\mathbf{I}^{i}_{index}$ (kW)	$\mathbf{I}^{i}_{index}/\lvert\Delta I^{i,calc}\rvert$%
Compressor	**538.8710**	**521.8509**	**17.0201**	**5.0010**	**12.0191**	**240.3339**
Air cooler	**812.0430**	**896.4213**	**-84.3783**	**-74.9410**	**9.4373**	**12.5930**
Cy 1	**1695.2112**	**1562.6779**	**132.5332**	**52.6593**	**79.8740**	**151.6808**
Cy 2	1647.2573	1563.0352	84.2220	83.1864	1.0356	1.2449
Cy 3	1647.9721	1563.0620	84.9101	83.6972	1.2129	1.4492
Cy 4	1647.6579	1563.0571	84.6008	83.9246	0.6762	0.8057
Cy 5	1647.2000	1563.0397	84.1603	83.2476	0.9127	1.0964
Cy 6	1647.1802	1562.9689	84.2113	83.1387	1.0726	1.2901
Turbine	**999.5440**	**976.3621**	**23.1819**	**-19.9771**	**43.1591**	**216.0422**

The diagnosis results of cases real 1–8 operating conditions are listed in Tables 10−17, in which each row referring to the malfunctioning components is highlighted in bold.

For example, looking at Table 10, first, it is worth noting that all the failures are accurately located and identified. In particular, the expected irreversibility variation of all components is higher than 0, which means that the propagation of the induced effects caused by failures involves all components in the system.

In addition, it can be found in Table 16 that all the failures are accurately located and identified. However, this method cannot identify the type of failure (piston ring abnormal wear or fuel pump wear).

Focusing on the malfunctioning components (i.e., the compressors and air coolers), the value of the index $\mathbf{I}_{index}^{i}$ (see the last but one column in the table) is high. This means that the actual irreversibility of such components is noticeably different from the expected irreversibility, indicating that their characteristic curve has changed because of their intrinsic operation anomalies. In contrast, the corresponding values of index $\mathbf{I}_{index}^{i}$ for the other components are close to 0 (note that the non-zero value is mostly due to the error ε in the approximation of the derivative), which means that the actual irreversibility of these components is basically equal to the expected irreversibility, i.e., the components are affected by malfunction induced effects and their characteristic curves do not deviate from the original one.

Finally, since the exergy flow rate of different components of the diesel engine system varies greatly, the ratios $\mathbf{I}_{index}^{i}/|\Delta I^{i,calc}|$ that are reported in the last column of the table, are the more proper diagnostic indexes to take into consideration. Tables 9 to 16 show that this index amplifies the anomaly of the components in which the intrinsic malfunction occurs increasing the gap existing between these components and the others, which are affected only by the approximation error in the evaluation of the derivatives of the characteristic curves. Thus, this index greatly simplifies the failure location and identification process.

5. Conclusions

This paper proposes a diagnosis method for diesel engines based on the characteristic curve of each component. When multiple faults occur simultaneously in several different components, the advantage of this method is to effectively locate the malfunctions, so as to maintain the reliability of the system. The author establishes and verifies the reliable model of the 6S50 engine and each of its components, and then describes the characteristic curve of each component. On this basis, eight multiple malfunctions cases have been diagnosed and discussed to show the ability of the proposed method.

The following conclusions can be drawn from this application:

1) The validity and reliability of the method were demonstrated by eight test cases. The method is able to effectively isolate the propagation phenomena of faults in the system, and accurately identify the location of faults in the marine diesel engine system.

2) The author selected comprehensive and practical thermal performance parameters (that can be monitored) to describe the characteristic curves of the main components (compressor, turbine, cylinder and air cooler). Therefore, the proposed fault location method has high practical application value.

3) Both the irreversibility in the i^{th} component, $\mathbf{I}_{index}^{i}$ and $\mathbf{I}_{index}^{i}/|\Delta I^{i,calc}|$ and can be used as fault location indicators for the marine diesel engine system. Considering the exergy flow rate of different components of diesel engine systems varies greatly, it is more effective to choose $\mathbf{I}_{index}^{i}/|\Delta I^{i,calc}|$ as the fault location indicator.

4) The fault diagnosis method proposed in this paper can effectively locate malfunctions, but this method cannot identify the type of failure (piston ring abnormal wear or fuel pump wear). This method still needs to be combined with other fault identification methods to identify the type of failure.

Nomenclature	
Acronyms	
IMEP	Indicated Mean Effective Pressure (bar)
LHV	Lower Heating Value (J/kg)
Greek symbols	
Δ	Increment
π	dependent variable
δ	independent variable
ε	residual effects
γ	Density of fuel oil [g/(cm3)]
ρ	density
u	velocity of fluid
η	isentropic efficiency
Symbols	
I	Irreversibility
$\mathbf{I}_{\text{index}}$	Diagnostic index
E	Exergy flow
n	Diesel engine speed (rpm)
P	Diesel engine power (kW)
m	Mass flow rate (kg/s)
p	Pressure (bar)
T	Temperature (K)
$\boldsymbol{T}$	Torque (N·m)
f	characteristic curve function
W	Power (kW)
W_e	Nominal engine power (kW)
g_e	Fuel consumption rate g/(kW·h)
Δh	The amount of oil supplied per 100 cycles (ml)
n_e	Nominal engine speed (rpm)
D	Bore (mm)
S	Stroke (mm)
F	Failure type
C1	Air compressor
C2	Air cooler
C3~C8	Cylinder 1~6
C9	Turbine
L	Number of cylinders
t	time
x	means flow longitudinal dimension
e	means total internal energy
h	total enthalpy
R	gas constant
k	adiabatic exponent air

Continued on next page

Nomenclature	
Subscripts	
MP	Measure point location
ref	reference operating condition
real	real operating condition
C	Compressor
T	Turbine
xa	air exergy flow
xg	gas exergy flow
xf	fuel exergy flow
xq	cooling water exergy flow
calc	calculated
i	Index for numerating of components

Conflict of interest

The authors declare there is no conflict of interest.

References

1. V. T. Lamaris, D. T. Hountalas, A general purpose diagnostic technique for marine diesel engines–Application on the main propulsion and auxiliary diesel units of a marine vessel, *Energy Convers. Manage.*, **51** (2010), 740–753. https://doi.org/10.1016/j.enconman.2009.10.031
2. D. W. Wang, L. Shi, S. P. Zhu, B. Liu, Y. H. Qian, K. Y. Deng, Numerical and thermodynamic study on effects of high and low pressure exhaust gas recirculation on turbocharged marine low-speed engine, *Appl. Energy*, **261** (2020), 114346. https://doi.org/10.1016/j.apenergy.2019.114346
3. J. Carlton, J. Aldwinkle, J. Anderson, *Future Ship Powering Options: Exploring Alternative Methods of Ship Propulsion*, London: Royal Academy of Engineering, 2013.
4. Brent, Haight, 2011 marine propulsion order survey: a review of mechanical drive, auxiliary and diesel-electric marine propulsion orders in 2010, *Diesel & Gas Turbine Worldwide*, **43** (2011), 30–30.
5. A. Jardine, D. Lin, D. Banjevic, A review on machinery diagnostics and prognostics implementing condition-based maintenance, *Mech. Syst. Signal Process.*, **20** (2006), 1483–1510. https://doi.org/10.1016/j.ymssp.2005.09.012
6. J. Galindo, J. R. Serrano, F. Vera, C. Cervello, M. Lejeune, Relevance of valve overlap for meeting Euro 5 soot emissions requirements during load transient process in heavy duty diesel engines, *Int. J. Veh. Des.*, **41** (2006), 343–367, https://doi.org/10.1504/IJVD.2006.009675
7. G. Vera, P. Rubio, H. Grau, Improvements of a failure database for marine diesel engines using the RCM and simulations, *Energies*, **13** (2019), 104. https://doi.org/10.3390/en13010104
8. A. Jose, V. G. Francisco, H. G. Jose, M. C. Jose, A. H. Daniel, Marine diesel engine failure simulator based on thermodynamic model, *Appl. Therm. Eng.*, **144** (2018), 982–995. https://doi.org/10.1016/j.applthermaleng.2018.08.096
9. R. Pawletko, S. Polanowski, Evaluation of current developments and trends in the diagnosis of marine diesel engines based on the indicator diagrams analysis, *J. KONES,* **21**(2014), 389–396. https://doi.org/10.5604/12314005.1130492

10. A. J. Bayba, D. N. Siegel, K. Tom, *Application of Autoassociative Neural Networks to Health Monitoring of the CAT 7 Diesel Engine*, *Army Research Laboratory*, 2012.
11. D. T. Hountalas, Prediction of marine diesel engine performance under fault conditions, *Appl. Therm. Eng.*, **20** (2000), 1753–1783. https://doi.org/10.1016/S1359-4311(00)00006-5
12. J. Rubio, F. Vera-García, *Sistema de Diagnóstico de Motor Diesel Marino Basado en Modelo Termodinámico y de Inteligencia Artificial*, Ph.D thesis, Universidad Politécnica de Cartagena, 2017. https://doi.org/10.13140/RG.2.2.32226.63688
13. X. W. Li, Study on fault diagnosis of narine diesel engine, *Comput. Simul.*, **12** (2012), 21–32. https://doi.org/10.1108/eb052507
14. Z. Jian, Simulation research on EGR reducing No_x emission of diesel engine, *Int. J. Energy Power Eng.*, **4** (2015), 275–279. https://doi.org/10.11648/j.ijepe.20150405.16
15. C. Iclodean, N. Burnete, Computer simulation of ci engines fuelled with biofuels by modelling injection iRate law, *Res. J. Agric. Sci.*, **44** (2012), 249–257.
16. T. Firsa, AVL Boost simulation of engine performance and emission for compressed natural gas direct injection engine, *J. Energy Environ.*, **6** (2014).
17. O. C. Basurko, Z. Uriondo, Condition-Based maintenance for medium speed diesel engines used in vessels in operation, *Appl. Therm. Eng.*, **80** (2015), 404–412. https://doi.org/10.1016/j.applthermaleng.2015.01.075
18. G. Qi, Z. Zhu, K. Erqinhu, Y. Chen, Y. Chai, J. Sun, Fault-diagnosis for reciprocating compressors using big data and machine learning, *Simul. Modell. Pract. Theory*, **80** (2018), 104–127. https://doi.org/10.1016/j.simpat.2017.10.005
19. Z. Zhu, Y. Lei, G. Qi, Y. Chen, Y. Chai, Y. An, et al., A review of the application of deep learning in intelligent fault diagnosis of rotating machinery, *Measurement*, **206** (2022), 112346. https://doi.org/10.1016/j.measurement.2022.112346
20. X. Huang, G. Qi, N. Mazur, Y. Chai, Deep residual networks-based intelligent fault diagnosis method of planetary gearboxes in cloud environments, *Simul. Modell. Pract. Theory*, **116** (2022), 102469. https://doi.org/10.1016/j.simpat.2021.102469
21. V. Kneevi, J. Orovi, L. Stazi, J. Ulin, Fault tree analysis and failure diagnosis of marine diesel engine turbocharger system, *J. Mar. Sci. Eng.*, **8** (2020), 1004. https://doi.org/10.3390/jmse8121004
22. Z. Jiang, D. Wei, L. Wang, Z. Zhao, J. Zhang, Fault diagnosis of diesel engines based on a classification and regression tree (CART) decision tree in Chinese, *J. Beijing Univ. Chem. Technol.*, **45** (2018), 71–75. https://doi.org/10.13543/j.bhxbzr.2018.04.013
23. F. Elamin, Y. Fan, F. Gu, A. Ball, Diesel engine valve clearance detection using acoustic emission, *Advances in Mechanical Engineering*, **2** (2010), 495741. https://doi.org/10.1155/2010/495741
24. K. Chen, Z. Mao, H. Zhao, J. Zhang, A variational stacked autoencoder with harmony search optimizer for valve train fault diagnosis of diesel engine, *Sensors*, **20** (2019), 223. https://doi.org/10.3390/s20010223
25. A. Valero, C. Torres, L. Serra, A general theory of thermoeconomics. Part I: Structural analysis, in *1992 International Symposium ECOS*, ASME, New York, USA, (1992), 137–145.
26. A. Valero, C. Torres, F. Lerch, Structural theory and thermoeconomic diagnosis. Part III: intrinsic and induced malfunctions, in *1999 International Symposium ECOS*, ASME, New York, USA, (1999), 8–10.

27. A. Valero, C. Torres, L. Serra, Structural theory and thermoeconomic diagnosis. Part I: On malfunction and dysfunction analysis, *Energy Convers. Manage.*, **43** (2002), 1503–1518. https://doi.org/10.1016/S0196-8904(02)00032-8
28. A. Valero, M. A. Lozano, J. L. Bartolomé, On-line monitoring of power-plant performance, using exergetic cost techniques, *Appl. Therm. Eng.*, **16** (1996), 933–948. https://doi.org/10.1016/1359-4311(95)00092-5
29. A. Valero, F. Lerch, L. Serra, Structural theory and thermoeconomic diagnosis. Part II: Application to an actual power plant, *Energy Convers. Manage.*, **43** (2002), 1519–1535. https://doi.org/10.1016/S0196-8904(02)00033-X
30. V. Vittorio, L. M. Serra, V. Antonio, Effects of the productive structure on the results of the thermoeconomic diagnosis of energy systems, *Int. J. Thermodyn.*, **5** (2002), 127–137. https://doi.org/10.5541/ijot.95
31. V. Vittorio, L. M. Serra, A. Valero, Zooming procedure for the thermoeconomic diagnosis of highly complex energy systems, *Int. J. Thermodyn.*, **5** (2002), 75–83. https://doi.org/10.5541/ijot.90
32. V. Vittorio, L. M. Serra, V. Antonio, The effects of the control system on the thermoeconomic diagnosis of a power plant, *Energy*, **29** (2004), 331–359. https://doi.org/10.1016/j.energy.2003.10.003
33. A. Stoppato, A. Lazzaretto, Exergetic analysis for energy system diagnosis, in *1996 Biennial Joint Conference on Engineering Systems Design and Analysis*, ASME, New York, USA, (1996), 191–198.
34. A. Lazzaretto, A. Toffolo, A critical review of the thermoeconomic diagnosis methodologies for the location of causes of malfunctions in energy systems, *J. Energy Res. Technol.*, **128** (2003), 345–354. https://doi.org/10.1115/1.2358148
35. A. Stoppato, C. Carraretto, A. Mirandola, A diagnosis procedure for energy conversion plants: Part I—Description of the method, in *ASME International Mechanical Engineering Congress and Exposition*, American Society of Mechanical Engineers, New York, USA, (2001), 493–500. https://doi.org/10.1115/IMECE2001/AES-23658
36. A. Stoppato, C. Carraretto, A. Mirandola, A diagnosis procedure for energy conversion plants: Part II—Application and results, in *ASME International Mechanical Engineering Congress and Exposition*, American Society of Mechanical Engineers, New York, USA, (2001), 501–508. https://doi.org/10.1115/IMECE2001/AES-23659
37. A. Toffolo, A. Lazzaretto, A new thermoeconomic method for the location of causes of malfunctions in energy systems, *J. Energy Res. Technol.*, **129** (2007), 1–9. https://doi.org/10.1115/1.2424960
38. A. Lazzaretto, A. Toffolo, R. Passuello, The characteristic curve method in energy systems diagnosis: analysis of uncertainties in a real plant, in *ASME International Mechanical Engineering Congress and Exposition*, ASME, New York, USA, (2005), 379–390.
39. AVL BOOST Theory Reference, v2020. Available from: https://www.avl.com/en/search.
40. H. M. Nahim, R. Younes, H. Shraim, M. Ouladsine, Oriented review to potential simulator for faults modeling in diesel engine, *J. Mar. Sci. Technol.*, **21** (2016), 533–551. https://doi.org/10.1007/s00773-015-0358-6
41. G. Radica, Expert system for diagnosis and optimisation of marine diesel engines, *Strojarstvo*, **50** (2008), 105–116.

42. P. Karpiński, K. Pietrykowski, L. Grabowski, Turbocharging the aircraft two-stroke diesel engine, *Combust. Engines*, **178** (2019). https://doi.org/10.19206/CE-2019-319
43. G. Cong, T. Gerasimos, C. Hui, Analysis of two stroke marine diesel engine operation including turbocharger cut-out by using a zero-dimensional model, *Energies*, **8** (2015), 5738–5764. https://doi.org/10.3390/en8065738
44. L. Wang, P. Fu, N. Wang, T. Morosuk, Y. Yang, G. Tsatsaronis, Malfunction diagnosis of thermal power plants based on advanced exergy analysis: The case with multiple malfunctions occurring simultaneously, *Energy Convers. & Manage.*, **148** (2017), 1453–1467. https://doi.org/10.1016/j.enconman.2017.06.086

AIMS Press